Journal of Applied Fluid Mechanics, Vol. 18, No. 5, pp. 1140-1157, 2025.
Available online at www.jafmonline.net, ISSN 1735-3572, EISSN 1735-3645.
https://doi.org/10.47176/jafm.18.5.3126

A Simulation of Bubbly Flow Regime in Boiling Process by Comparing the Numerical Models of VOF and RPI Boiling

S. Torfeh[1], M. Mirzaei[1] and R. Kouhikamali[2†]

[1] *Faculty of Mechanical Engineering, University of Guilan, Rasht, Guilan, 4199613776, Iran*
[2] *Department of Mechanical Engineering, Isfahan University of Technology, Isfahan, 8415683111, Iran*

†*Corresponding Author Email: r.kouhikamali@iut.ac.ir*

ABSTRACT

Boiling process in a heated tube is commonly used in different industries such as electronic equipment cooling, power plant, and air conditioning systems. Despite the significance of thoroughly and separately analyzing of heat transfer in different two-phase flow regimes encountered in boiling process, just a few simulations have been conducted. That is because of the lack of proper understanding of the many numerical methods that are now in use and their relative efficacy under various circumstances. This leads to dispersed effort and the application of disparate numerical methods, which incurs significant computational expenses. In this study, Eulerian-Eulerian approach was used to simulate the bubbly flow, which includes vapor bubbles in the rising water flow within a vertical tube. In order to identify the optimal numerical model and the extent of application of available numerical models in the simulation of bubbly flow, volume of fluid (VOF) and Eulerian boiling model of Rensselaer Polytechnic Institute (RPI) models were compared and evaluated. Results demonstrated that while the RPI boiling model results are more appropriate for estimating the heat transfer coefficient and wall temperature in this regime, the VOF model is more effective than the RPI model at simulating the regime, bubble formation and interface between phases. Moreover, RPI model was used to examine how changes in wall heat flux and inlet mass flow rate affected effective parameters. Results revealed that in the bubbly flow regime, a 100% increase in wall heat flux relative to its original value of 5000 W/m^2, resulted in a 150% increase in the outlet vapor quality, a 75% rise in temperature difference between the wall and the saturation temperature, and a 20.8% increase in the mean wall heat transfer coefficient. Furthermore, by increasing the inlet mass flow rate, the nucleate boiling zone increases and the outlet vapor quality decreases.

Article History

Received September 11, 2024
Revised December 28, 2024
Accepted December 31, 2024
Available online March 4, 2025

Keywords:

Numerical simulation
Eulerian-Eulerian approach
Volume of fluid
RPI boiling
Heat transfer mechanism

1. INTRODUCTION

Power plants, petrochemical, heating and cooling equipments, as well as refinery processes frequently employ boiling process. Nowadays, the optimization of energy consumption in the design and construction of heat exchangers, especially evaporators, is of major importance due to the constraint of energy resources and the necessity to preserve energy, which leads to a thorough analysis and study of this process. The precise two-phase flow regimes generated during this operation, as well as the heat transfer mechanism in each of these regimes, must be known for this study. The boiling phenomenon initiates with the development of gas bubbles near the tube wall and terminates with the creation of a vapor phase. Until the temperature of the liquid and the wall are both below the saturation temperature of the liquid, the heat transfer to the liquid during the initial stages of this process is a single-phase convective heat transfer. Boiling starts when the temperature reaches the saturation temperature, depending on the wall properties and operational circumstances. In this condition, if the bulk liquid temperature is still below the saturation temperature, subcooled boiling occurs and when the bulk of the liquid reaches its saturation temperature and the wall temperature exceeds the saturation point, saturated boiling is detected. The vapor quality or vapor mass fraction in this instance ranges from 0 to 1 (Kandlikar, 1999). The flow regime in saturated boiling varies as the quality of the vapor increases. The bubbly flow regime, which manifests

NOMENCLATURE

A_b	penetration area	q_E	evaporative heat flux
c_p	specific heat	$\bar{R}_{pq}$	interphase force
D	tube diameter	Re	Reynolds number
D_ω	bubble departure diameter	S	source term
E	energy	t	time
F_{lift}	lift force	T	temperature
F_q	external body force	u, v	velocity
F_{vm}	virtual mass force	V	volume
f	frequency of bubble departure	x	vapor quality
g	gravitational acceleration	X_{tt}	Martinelli coefficient
G	total mass flux	α	volume fraction
H	specific enthalpy	ε	dissipation rate
h	heat transfer coefficient	$\bar{\bar{\tau}}$	stress-strain tensor
h_c	convective heat transfer coefficient	κ	turbulence kinetic energy
h_{NcB}	nucleate boiling heat transfer coefficient	λ	bulk viscosity
I_t	turbulence intensity	μ	shear viscosity
k	conductivity	ρ	density
K	experimental constant in penetration area equation	σ	surface tension
l	turbulence length scale	ϕ	shape factor
L	tube length	bp	boiling point
M	molecular weight	l	liquid
$\dot{m}$	mass flow rate	v	vapor
Nu	Nusselt number	i	inlet
N_ω	local nucleate density	o	outlet
P	pressure	p	phase p
P_r	reduced pressure	q	phase q
Pr	Prandtle number	Sat	saturation
q	wall heat flux	w	wall
q_c	convective heat flux		

as small vapor bubbles in the tube, forms upon early in the flow when the vapor quality is low. The size of the bubbles gradually grows as the quality of the vapor increases, and the pattern and flow regimes vary as the distribution of the interface between the two phases of vapor and liquid changes. Each two-phase flow regime has its own hydrodynamic and heat transfer properties (Collier & Thome, 1996).

Saturated boiling, which primarily involves nucleate boiling heat transfer, is the predominant heat transfer mechanism in the bubbly flow regime. Since evaluation of the fluid behavior and investigation of the bubbles formation and departure from the surface are very complicated; convective and nucleate boiling analysis and modeling are difficult tasks too. As a thorough understanding of the heat transfer mechanism in two-phase flow is essential to investigate boiling process in different industries; numerous experimental researches have been conducted in this field under various conditions, and also several empirical correlations have been proposed.

Chen (1966) originally proposed a correlation that is regarded as the first common equation for estimating the heat transfer coefficient in the saturated boiling process in vertical tubes utilizing 600 experimental data collected for water, cyclohexane, and pentane. This correlation has a large inaccuracy for other refrigerants, but it is rather accurate for water fluid at low pressures. Shah (1982, 2006) created a diagram to determine the heat transfer coefficient by modifying the dimensionless parameters of the Martinelli coefficient and boiling number more than ten years after Chen. The usefulness of his study was increased by the over 800 experimental data he obtained for water with pressures ranging from 15 to 2500 psi and several common refrigerants in various heat and mass fluxes for the boiling process in vertical and horizontal tubes. Gungor and Winterton (1986) proposed a modified correlation for boiling in a tube using around 4300 experimental data for different refrigerants, ethylene glycol, and water by combining the correlations of Chen (1966) and Shah (1982). The mean inaccuracy of this correlation is 21.4% for saturated boiling, and 25% for subcooled boiling. Kandlikar (1999, 1990) developed an experimental correlation for determining the heat transfer coefficient based on 10,000 experimental data for water, several types of refrigerants, and refrigerant mixtures for a wide range of density ratio, heat flux, and mass flux.

Another group of studies have been focused on conducting experiments to examine the geometry or particular parameters effects on bubbly flow regime. In recent years, numerical analyses and modeling have also attracted a lot of interest as the design, development, and optimization of heat exchangers and evaporators depend

on numerical simulations with the proper estimation of experimental works.

Mizushina et al. (1968) studied the bubbly flow including water and air bubbles in evaporative cooling tube bundles. As demonstrated in this study, the heat transfer coefficient between the water and the tube in this regime is significantly larger than the flow of a falling film on a horizontal tube. Despite the high heat transfer coefficient under these conditions, the drastic drop in air pressure and increased pump requirements make evaporative coolers an uneconomical mechanism. Son (2001) provided a model that is based on the level adjustment approach and can demonstrate the impacts of phase change and attaining mass balance in the interphase surface to simulate the initiation and growth of bubbles in a static fluid. Ye et al. (2001) enhanced the direct numerical simulation method simultaneously with Son (2001), and employed it to investigate the phase change and bubble shape change. The algorithm they described has demonstrated adequate accuracy in a wide range of Reynolds, Weber, Peclet, and Jacobian numbers. As a result, the balance of mass, momentum, and energy have been established in the interface, and the associated equations have been solved using the finite volume approach.

Pang et al. (2010) studied the rising bubbly flow in a vertical channel with two parallel planes using the Eulerian-Lagrangian method. They investigated the impacts of air bubbles injection on the fluid turbulence. They found that the drag force has the maximum impact on the fluid flow and the lift force determines how close the bubbles are to the wall. By displaying the volume fraction diagram, they showed that the most steam can be seen in the vicinity of the walls.

Lim and Yu (2014) examined the characteristics of heat transfer in a symmetrical air-water two phase flow in micro-tubes with inner diameters of 300 and 500 micrometers using numerical modeling. They produced the two-phase flow by axially injecting nitrogen gas into the continuous liquid phase flow through an axial tube. The bubbly flow findings from the experiments and the bubbly flow results from the numerical simulation were compared by applying a uniform heat flux on the wall. They compared the heat transfer process results in the two-phase flow and single-phase liquid flow. Results demonstrated that the Nusselt number in two-phase flow grows up to 200%, while the two-phase frictional pressure drop for bubbly flow is approximately 20% greater than liquid flow. Attarakih et al. (2016) conducted a numerical investigation of the air-water bubbly flow in a vertical tube. A novel approach named OPOSPM and its coupling with the Eulerian two-fluid model (TFM), which was not capable of accurately simulating the decomposition and merging of bubbles, was introduced to fill the gap in the simulation. This was essential since the interactions of liquid and gas phases as well as bubble-bubble interactions are significant in growth, collapse and merging of bubbles in the bubbly flow regime. They also compared the numerical results with actual experimental data.

Monferrer et al. (2018) neglected the processes of bubbles coalescence and breakup to examine the dynamics of bubbles and their interaction with the fluid phase in detail. However, they were able to investigate the motion of each bubble independently and take into account parameters like inhomogeneity, nonlinearity of the interfacial forces, bubble-wall interactions and turbulence effects in interfacial forces after developing the two-fluid numerical model by combining the solver with the discrete element method (DEM). They compared the results of experiments conducted for bubbly flow in a vertical tube with their examined models for assignment of void fraction into the grid, seeding of bubbles at the inlet, pressure change influence on the bubble size and turbulence effects on both phases. In keeping with the hydrodynamic study of bubbly flow, Zhang et al. (2020) also presented an enhanced multi-scale two-phase solution for bubbly flow simulation, whereby the Eulerian-Lagrangian method was used to model micro-scale bubbles and the volume of fluid method was used to simulate macro-scale bubbles. Two-way coupling in Lagrangian tracking was considered in this study for investigating of the motions, collisions, coalescence and breakup of bubbles, as well as the mutual interaction of phases. The results of the enhanced multi-scale and the volume of fluid model for simulating bubble movement were thus compared.

Etminan et al. (2021a) investigated the hydrodynamics of air-water two-phase flow in an axisymmetric microchannel. Volume of Fluid model was employed to simulate Taylor flow in order to predict the interfacial phenomena between phases. Film thickness, bubble curvature, pressure drop, bubble/slug lengths were determined to investigate gas-liquid Taylor flow in micro capillaries. They validated their numerical results with theoretical and experimental available data which showed good agreement. Furthermore, Etminan et al. (2021b) presented a comprehensive review of hydrodynamics, flow patterns, and liquid film thickness in two-phase flows through mini and micro channels with different cross-sectional geometry. Their paper also reviewed correlations that predict liquid film thickness in micro channels for gas-liquid and liquid-liquid flows.

Zhang et al. (2023) used a hybrid thermal multiphase model that included pseudopotential multiphase lattice Boltzmann model and the finite difference method to investigate boiling heat transfer in a serpentine microchannel. This study analyzed how the curvature ratio, flow direction, heat flux, and Reynolds number affected the performance of heat transfer and bubble dynamic behavior during the flow boiling process. The simulations results demonstrated that while increasing the curvature ratio elongated bubbles at the U-bend, it does not affect heat transfer efficiency. The buoyancy resulting from the gravity acceleration had both positive and negative impacts on the local heat transfer characteristics and bubble dynamic behaviors in the serpentine microchannel, depending on the direction of flow. They also calculated the vapor volume fraction for various heat fluxes and Reynolds numbers. Zhou et al. (2023) used a volume of fluid model to numerically simulate the bubble dynamics and heat transfer characteristics of boiling

process in a pentagonal rib channel for the cooling of electronic equipment. They analyzed how the length-diameter ratios, flow Reynolds number, and heat flux affected the process of bubble formation, wall temperature and temperature fluctuations, and heat transfer coefficient. The findings demonstrated that the bubble originates at the cone and sides of the rib, and heat flux and fluid velocity influence the direction of the bubbles movement. Furthermore, by increasing the heat flux and decreasing the fluid velocity, the wall temperature and temperature fluctuations increase.

Igaadi et al. (2023) investigated the thermal performance, pressure drop, and flow patterns behavior of subcooled flow boiling in different configurations of a vertical mini channel for several mass fluxes. A 2D numerical simulation was performed using the volume of fluid model. A new periodic constriction-expansion design was studied and compared to the straight mini channel to determine the appropriate configuration that enhances heat transfer.

Mughal et al. (2024) studied the heat transfer performance of mini channels in a water-steam system using the Volume of Fluid model coupled with the Lee phase change model. A 3D simulation was performed and the effects of mass flux and heat flux on the heat transfer coefficient were analyzed. They showed that this model can be applied to design two-phase heat transfer systems such as steam generators with reasonable accuracy.

Reviewing the related literature in this area reveals that the majority of numerical studies in this field focus on hydrodynamics and gas-liquid bubbly flow patterns, and the modeling of generated gas bubbles dynamics, while excluding the mass transfer and phase change processes. Additionally, the process of boiling and heat transfer in two-phase flows have been mostly studied experimentally to provide new empirical correlations or to modify existing ones. Despite the significance of thoroughly and separately analyzing of the heat transfer mechanism in different two-phase flow regimes encountered in the boiling process, just a few simulations have been conducted. One of the reasons of this is a lack of proper understanding of the many numerical methods that are now in use and their relative efficacy under various circumstances. This leads to dispersed effort and the application of disparate numerical methods for even identical numerical works, which incurs significant computational expenses. As a result, the current study uses an Eulerian-Eulerian approach to numerically simulate the bubbly flow regime in a vertical tube while considering the mass transfer resulting from phase change in saturated boiling. To identify the optimal numerical method and the range of applications for each in this regime, two numerical models including volume of fluid (VOF) and Eulerian boiling from Rensselaer Polytechnic Institute (RPI) have been compared and evaluated in this modeling. Furthermore, one of the primary objectives of this research is to verify that the modeling and investigation of heat transfer in this regime be accurate. Another objective of this research is to investigate the effects of the wall heat flux and incoming mass flux changes on the heat transfer coefficient and volume fraction of vapor in the flow of boiling water in a vertical tube using the selected numerical method. Thus, the status of heat transfer in this regime within the evaporators with vertical tubes can be precisely studied with the aid of the research findings.

2. FUNDAMENTALS OF NUMERICAL SIMULATION OF TWO-PHASE BUBBLY FLOW

To select the appropriate numerical method and its applicability for each of the two-phase regimes, a comprehensive understanding of the current numerical models and their governing equations is necessary. In this study, two methods including VOF and Eulerian boiling of RPI from the Eulerian-Eulerian approach were compared and evaluated to get the most accurate numerical solution method and simulation of fluid flow with the least amount of inaccuracies. Volume fraction of each phase is used to compute the flow parameters in the VOF model, which represents the multi-phase flow as a single-phase virtual flow. In other words, every conservation equation for a multiphase flow is solved just once, with common properties arising from the volume fraction of each phase. The VOF model has several limitations, such as the requirement for the use of a separate equation solver and the inapplicability of a coupled equation solver for this particular model. Only one of the phases can be defined as a compressible ideal gas, otherwise, the flow must be regarded as incompressible. On the other hand, in bubbly flows, where vapor bubbles are dispersed in a liquid, the VOF method can accurately track the vapor-liquid interface, providing detailed insights of bubble formation, rise, coalescence, and breakup. Additionally, VOF allows for a sharp representation of the interface between the phases, which is essential in bubbly flows, where the bubbles maintain a distinct boundary from the surrounding liquid phase. Since bubbly flows can involve significant local variations in vapor volume fractions, the VOF method can effectively capture these variations without requiring excessive computational resources, as it focuses on volume fractions at each point rather than resolving every single bubble. However, the most comprehensive model for examining and evaluating two-phase or multiphase flows is the Eulerian model. This model has a greater simulation time and computational cost since the equations of mass, momentum, and energy conservation are calculated separately for each phase. In addition, RPI boiling model is specifically designed for simulating boiling phenomena, including the nucleation and growth of bubbles at heated surfaces. It accounts for the effects of temperature and surface interactions, which are crucial in bubbly flows, especially in boiling regimes where bubbles form from a heated liquid. The model incorporates heat transfer mechanisms related to bubble growth and the latent heat of vaporization, which are important when simulating systems such as boiling reactors, heat exchangers, and other boiling two-phase flow systems.

To clearly illustrate relevant details of the simulation setup, the schematic pattern for Eulerian-Eulerian two-phase flow simulation with heat transfer is presented, which typically involves the following stages:

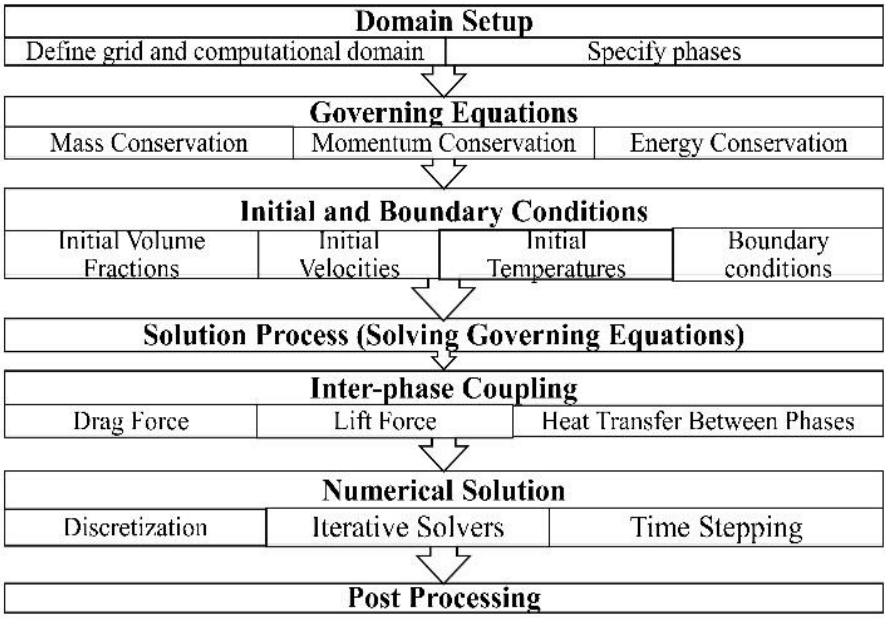

Fig. 1 Schematic illustration of the approach as a flow chart

• Domain Setup: Definition of a fixed computational domain with a grid. Both phases (e.g., liquid and vapor) are treated as interpenetrating continua.

• Initial and Boundary Conditions: Setting initial distributions for phase volume fractions, velocities, and temperatures. Boundary conditions for mass, momentum, and energy must also be specified. At boundaries (e.g., solid walls), no-slip conditions for velocity, temperature boundary conditions, and phase change conditions (e.g., boiling or condensation at solid-liquid interfaces) must also be specified as wall boundaries.

• Solution Process:

Phase 1 and Phase 2 are solved simultaneously, with heat transfer and phase interactions considered in the governing equations.

Iterative coupling is required to exchange heat between the phases at each time step.

- Solving the mass conservation equations for both phases.
- Solving the momentum equations for each phase.
- Solving the energy equations for each phase, considering heat transfer terms between phases.

Inter-phase Coupling: The phases interact through forces (like drag) and heat transfer, which are modeled as source terms in the equations.

Heat Transfer Between Phases:

- Conduction: Heat conduction occurs within each phase, based on the temperature gradients.
- Convection: Each phase transports heat due to the flow (convective heat transfer).
- Phase Change: If a phase change (e.g., evaporation or condensation) occurs, the latent heat of phase change is included in the energy balance.
- Interphase Heat Transfer: Heat exchange between the phases (e.g., between liquid and vapor) is modeled using heat transfer coefficients or empirical correlations, using models like the Nusselt number correlation for convective heat transfer and effective thermal conductivity for conduction.

• Turbulence Models: Depending on the flow regime, turbulence interaction between phases can be modeled using turbulence models.

• Numerical Solution: The solution is typically carried out using numerical methods like Finite Volume (FV) or Finite Difference (FD) methods. Iterative solvers, such as SIMPLE or PISO, are commonly used to handle the coupling between mass, momentum, and energy equations.

• Time Integration:

The system is solved iteratively in time using appropriate time-stepping schemes (e.g., explicit or implicit methods).

• Post-Processing:

Once the simulation is complete, temperature fields, heat flux distributions, and phase fraction profiles are extracted and analyzed.

Schematic illustration of the approach, as a flow chart for Eulerian-Eulerian two-phase flow with heat transfer is represented in Fig. 1 to visualize the problem more effectively.

3. GOVERNING EQUATIONS

3.1 VOF Model Equations for Two-Phase Flows

The VOF formulation relies on the fact that phases are not interpenetrating. In this model a variable called volume fraction (α) is introduced, which denotes the area

occupied by each phase in two or more immiscible fluids. The sum of total volume fractions in each control volume is equal to one. The fields for each of the variables and properties are shared by the phases and represent volume-averaged values, until the volume fraction of each phase is denoted at each location (Hirt & Nichols, 1981).

In this model, a continuity equation for the volume fraction of one or more phases is solved to track the interfaces between phases. This equation is expressed for the th phase using Eq. (1) (Hirt & Nichols, 1981; Mughal et al., 2024).

$$\frac{1}{\rho_q}\left[\frac{\partial}{\partial t}\left(\alpha_q\rho_q\right)+\nabla\cdot\left(\alpha_q\rho_q\vec{v}_q\right)=S_{\alpha_q}+\sum_{p=1}^{n}\left(\dot{m}_{pq}-\dot{m}_{qp}\right)\right] \tag{1}$$

The term S_{α_q} on the right side of Eq. (1) is the source term. Mass transfer between phases is also indicated by expressions $\dot{m}_{pq}$ and $\dot{m}_{qp}$. User-defined functions (UDF) for each phase are required to describe the mass transfer and source term. This method involves expressing all the properties as a function of the volume fraction of the phases. Equation (2) expresses the density in each cell if the phases are represented by subscripts 1 and 2 and if the volume fraction of each phase is tracked (Yang et al., 2022).

$$\rho=\alpha_2\rho_2+(1-\alpha_2)\rho_1 \tag{2}$$

This method shares the given velocity field among the phases by solving a single equation of momentum. One of the constraints of the approximation of the related fields is that the high-velocity difference between the phases affects the accuracy of the predicted velocities near the interface between the two phases. Equation (3) states that properties μ and ρ link the momentum equation to the volume fraction of each phase (Hasanpour et al., 2018; Mughal et al., 2024).

$$\frac{\partial}{\partial t}\left(\rho\vec{v}\right)+\nabla.\left(\rho\vec{v}\vec{v}\right)=-\nabla p+\nabla.\left[\mu\left(\nabla\vec{v}+\nabla\vec{v}^{T}\right)\right]+\rho\vec{g}+\vec{F}_{vol} \tag{3}$$

The energy equation, also shared among the phases, is indicated in Eq. (4) for incompressible fluids (Mughal et al., 2024).

$$\frac{\partial}{\partial t}\left(\rho E\right)+\nabla.\left(\vec{v}\left(\rho E+p\right)\right)=\nabla.\left(k_{eff}\nabla T\right)+S_h \tag{4}$$

where k_{eff} represents the effective thermal conductivity. Equations (5) and (6) are used to determine the energy E and heat source S_h which is caused by phase change.

$$E=\frac{\sum_{q=1}^{n}\alpha_q\rho_q E_q}{\sum_{q=1}^{n}\alpha_q\rho_q} \tag{5}$$

$$S_h=\dot{m}h_{fg} \tag{6}$$

E_q is calculated for each phase based on the specific heat of the phase and the shared mass-averaged temperature.

3.2 Eulerian Model Equations for Two-Phase Flows

Due to the persistent changes in the flow regime and mass transfer between the vapor and liquid phases, two-phase flows equations are far more complex than those for single-phase flows. In Eulerian model, the concept of volume fraction of phases is considered to characterize the multiphase flow as a continuous interpenetrating medium, and the laws of conservation of mass and momentum are satisfied for each phase separately. The derivation of the conservation equations can be done by ensemble averaging the local instantaneous balance for each of the phases or by using the mixture theory approach (Anderson & Jackson, 1967; Bowen, 1976).

V_q shows the volume of phase q in the Eulerian model, which is determined by Eq. (7).

$$V_q=\int\alpha_q dV \tag{7}$$

Thus, the volume fraction and effective density equations for phase q can be expressed using Eqs. (8) and (9), respectively (ANSYS FLUENT, 2017).

$$\sum_{q=1}^{n}\alpha_q=1 \tag{8}$$

$$\hat{\rho}=\alpha_q\cdot\rho_q \tag{9}$$

To determine the volume fraction of each cell in the Eulerian model for phase q, Eq. (8) and the continuity Eq. (10) are solved (ANSYS FLUENT, 2017).

$$\frac{\partial}{\partial t}(\alpha_q\rho_q)+\nabla\cdot(\alpha_q\rho_q\bar{v}_q)=\sum_{p=1}^{n}(\dot{m}_{pq}-\dot{m}_{qp})+S_q \tag{10}$$

$\dot{m}_{pq}$ is the mass transferred from phase p to the phase q and S_q is regarded as the mass source term in Eq. (10), where $\bar{v}_q$ stands for the velocity of phase q.

Each cell temperature is regarded as a value regardless of whether it is a single-phase or two-phase. When there is a phase change, the rate of condensation or evaporation is determined by the condensing and evaporating mass and the temperature difference between the cell temperature and the saturation temperature. Condensation and evaporation rates can be calculated using Eqs. (11) and (12).

$$T<T_{sat}\rightarrow \dot{m}_{pq}=r\alpha_p\rho_p\left(\frac{T_{sat}-T}{T_{sat}}\right),\dot{m}_{qp}=0 \tag{11}$$

$$T > T_{sat} \rightarrow$$
$$\dot{m}_{qp} = r\alpha_p\rho_p\left(\frac{T_{sat}-T}{T_{sat}}\right),\ \dot{m}_{pq} = 0 \tag{12}$$

In these equations, r is a coefficient that needs to be fine tuned and can be interpreted as a relaxation time, whose value varies based on each problem.

The momentum balance for phase q is shown in Eq. (13) and Eqs. (14) and (15) define parameters $\vec{v}_{pq}$ and $\vec{v}_{qp}$, which stand for interphase velocities (ANSYS FLUENT, 2017; Azadbakhti et al., 2020).

$$\frac{\partial}{\partial t}(\alpha_q\rho_q\vec{v}_q)+\nabla\cdot(\alpha_q\rho_q\vec{v}_q\vec{v}_q) = \alpha_q\nabla P+\nabla\cdot\bar{\bar{\tau}}_q+\alpha_q\rho_q\vec{g}+\sum_{p=1}^{n}(\vec{R}_{pq}+\dot{m}_{pq}\vec{v}_{pq}-\dot{m}_{qp}\vec{v}_{qp})+(\vec{F}_q+\vec{F}_{lift,q}+\vec{F}_{vm,q}) \tag{13}$$

$$\dot{m}_{pq} > 0 \ \rightarrow\ \vec{v}_{pq} = \vec{v}_p \tag{14}$$

$$\dot{m}_{pq} < 0 \ \rightarrow\ \vec{v}_{pq} = \vec{v}_q \tag{15}$$

Equation (16) represents parameter $\vec{R}_{pq}$. This parameter describes the interphase force, which is dependent on friction, pressure, cohesion, and other factors, and is a function of the interphase momentum exchange coefficient K_{pq}.

$$\sum_{p=1}^{n}\vec{R}_{pq} = \sum_{p=1}^{n}K_{pq}(\vec{v}_p-\vec{v}_q) \tag{16}$$

The external body force, lift force, and virtual mass force are represented by the parameters $\vec{F}_q$, $\vec{F}_{lift,q}$, and $\vec{F}_{vm,q}$ in the momentum equation, respectively. Except for situations when the phases are separated rapidly, the lift force is insignificant compared to the drag force. Equation (17) describes the impact of virtual mass force for multiphase flow, which occurs when the secondary phase accelerates, compared to the primary phase.

$$\vec{F}_{vm} = 0.5\rho_p\alpha_q\left(\frac{d_q(\vec{v}_p)}{dt}-\frac{d_p(\vec{v}_p)}{dt}\right) \tag{17}$$

The inertia of the first phase mass encountered by the accelerating bubbles exerts a virtual mass force on the bubbles. Accordingly, the virtual mass effect becomes significant when the secondary phase density is substantially lower than the density of the primary phase, where $\vec{F}_{vm,q} = -\vec{F}_{vm,p}$. The stress-strain tensor of phase q, denoted by parameter $\bar{\bar{\tau}}_q$ in Eq. (13), is defined as Eq. (18), where λ_q and μ_q stand for bulk and shear viscosity, respectively.

$$\bar{\bar{\tau}}_q = \alpha_q\mu_q(\nabla\vec{v}_q+\nabla\vec{v}_q^T)+\alpha_q\left(\lambda_q-\frac{2}{3}\mu_q\right)\nabla\cdot\vec{v}_q\bar{\bar{I}} \tag{18}$$

Equation (19) represents the energy equation for phase q in the Eulerian model and is expressed and computed independently for every phase (Azadbakhti et al., 2020).

$$\frac{\partial}{\partial t}\left(\alpha_q\rho_qH_q\right)+\nabla.\left(\alpha_q\rho_q\vec{v}_qH_q\right) = \alpha_q\frac{\partial P_q}{\partial t}+\bar{\bar{\tau}}_q+\nabla.\vec{v}_q-\nabla.\vec{q}_q+S_q+\sum_{p=1}^{n}\left(Q_{pq}+\dot{m}_{pq}H_{pq}-\dot{m}_{qp}H_{qp}\right) \tag{19}$$

In this equation, the parameters S_q, q_q, H_q, and Q_{pq} represent source term, heat flux, the specific enthalpy of phase q, and interphase heat exchange, respectively. Equation (20) defines the internal energy balance of the phase q in terms of the enthalpy terms of the main and secondary phases.

$$H_q = \int c_{p,q}dT \tag{20}$$

where $c_{p,q}$ represents phase q specific heat at constant pressure. Equation (21) states that the rate of heat exchange between phases is a function of temperature difference.

$$Q_{pq} = h_{pq}(T_p-T_q) \tag{21}$$

The Nusselt number of phase p, represented by Nu_p, determines the heat transfer coefficient h_{pq} between phases p and q based on Eq. (22).

$$h_{pq} = \frac{6k_q\alpha_p\alpha_qNu_p}{D_p^2} \tag{22}$$

The thermal conductivity of phase q is denoted by k_q in this equation. Typically, the experimental correlations are used to calculate the Nusselt number. Equation (23) states that the Runz and Marshall equation can be used in the fluid-fluid multiphase cases (Torfeh & Kouhikamali, 2015).

$$Nu_p = 2+0.6\,\mathrm{Re}_p^{\frac{1}{2}}\,\mathrm{Pr}^{\frac{1}{3}} \tag{23}$$

Where Pr is the Prandtl number and Re_p is the relative Reynolds number based on the diameter of p[th] phase and the relative velocity of the two phases.

A subset of the Eulerian model known as the boiling model for two-phase flow is employed in the current numerical simulation. The boiling model also comprises three subcategories including non-equilibrium subcooled boiling, critical heat flux, and RPI boiling. The RPI boiling model has been chosen based on the saturated boiling condition and the circumstances of the current problem. The energy is mostly transmitted directly from the wall to the fluid during the boiling process. Some of this energy raises the fluid temperature, some of it produces vapor, and some of it can be transferred directly from the wall to the generated vapor. The fluid mean temperature rises due to interphase heat transfer even when there is partial condensation of the bubbles. The RPI model is based on

these heat transfer mechanisms. RPI nucleate boiling, as proposed by Kural and Podowski (1991), and the deviation model from nucleate boiling, as proposed by Lavieville et al. (2006), models the wall boiling phenomenon.

In this model, three components including the evaporative heat flux (q_E), the quenching heat flux (q_Q), and the convective heat flux (q_C) constitute the heat energy (q_W) transferred from the wall to the fluid (Azadbakhti et al., 2020; Wu et al., 2023). The definition of the convective heat flux is given by Eq. (24). The single-phase heat transfer coefficient (h_C), the wall temperature (T_w), and the inlet fluid temperature (T_L) are the variables in this equation.

$$q_C = h_C(\mathrm{T}_w - \mathrm{T}_L)(1-\mathrm{A}_b) \tag{24}$$

Additionally, the heated surface of the wall is divided into two regions. Region A_b , which is covered with bubbles formed by nucleate boiling, and region $(1-\mathrm{A}_b)$, which is covered with liquid phase. The local nucleate density and the deviation diameter are the two parameters used in Eq. (25) to express the penetration area A_b (Wu et al., 2023).

$$A_b = \min(1, K\frac{N_w \pi D_w^2}{4}) \tag{25}$$

The experimental constant K in the Eq. (25) ranges from 1.8 to 5. The local nucleate density, N_w , is commonly described as Eq. (26).

$$N_w = C^n(T_w - T_{sat})^n \tag{26}$$

Equation (26) considers constant values for $n=1.8$ and $C=210$ based on the experimental correlations (Wu et al., 2023). In addition, D_w stands for the bubbles departure diameter, which is determined using Eq. (27).

$$D_w = \min(0.0014, 0.0006e^{-\frac{\Delta T_w}{45}}) \tag{27}$$

q_Q simulates the mean cyclic energy transfer related to the liquid film adjacent to the wall following the separation of the vapor bubbles which is represented in Eq. (28). Here, t_c is the cycle time, k_L represents the heat conduction, and, based on Eq. (29), λ_L expresses the penetration term.

$$q_Q = \frac{2k_L}{\sqrt{\pi \lambda_L t_c}}(T_w - T_L) \tag{28}$$

$$\lambda_L = \frac{k_L}{\rho_L c_{p_L}} \tag{29}$$

Equation (30) is also used to compute the evaporative heat flux q_E .

$$q_E = V_d N_w \rho_v h_{lv} f \tag{30}$$

In this equation, V_d , ρ_v , h_{lv} , and f represent the vapor bubbles volume, vapor density, latent heat of vaporization, and vapor departure frequency, respectively. Equation (31) defines the frequency of bubble departure in this equation (Wu et al., 2023).

$$f = \frac{1}{t_c} = \sqrt{\frac{4g(\rho_l - \rho_v)}{3\rho_l D_w}} \tag{31}$$

3.3 The Empirical Correlations to Calculate Heat Transfer Coefficient in Boiling Process

Chen (1966) and Gungor and Winterton (1986) correlations are empirical models used to predict the heat transfer coefficient in two-phase flow, typically for refrigerants or other fluid mixtures. Both correlations are widely used in the heat exchanger design and thermal analysis.

However, the accuracy of these correlations can vary depending on the flow conditions, fluid properties, and other factors. Generally, the errors associated with the Chen and Gungor & Winterton correlations are reported to be within certain limits.

3.3.1 Chen Correlation

Chen correlation is often used for the prediction of heat transfer coefficients in refrigerant and water flow under turbulent conditions. The error in predicting the heat transfer coefficient using the Chen correlation is typically reported to be in the range of ±15% to ±30% depending on the specific conditions and the quality of the data used in the experiment. In some cases, the error can be even higher under non-ideal or extreme conditions (e.g., very low mass flux or highly saturated fluid).

Chen & Fang (2014) used Eq. (32) to obtain the heat transfer coefficient by combining nucleate boiling and convection. He used the dimensionless parameter $\hat{F}$ in Eq. (33), which connected the convective heat transfer coefficient to the liquid phase heat transfer coefficient.

$$h_{TP} = h_{NcB} + h_c \tag{32}$$

$$h_C = 0.023\left[\frac{G(1-x)D}{\mu_l}\right]^{0.8}\left[\frac{\mu c_p}{k}\right]_l^{0.4}\left[\frac{k_l}{D}\right]\cdot \hat{F} \tag{33}$$

Chen presented the diagram in Fig. 2 to calculate the $\hat{F}$ parameter. He demonstrated how the dimensionless parameter $\hat{F}$ is dependent on the Martinelli coefficient. Note that Eq. (34) is used to determine the Martinelli coefficient.

$$X_{tt} = \left[\frac{(1-x)}{x}\right]^{0.9}\left[\frac{\rho_v}{\rho_l}\right]^{0.5}\left[\frac{\mu_l}{\mu_v}\right]^{0.1} \tag{34}$$

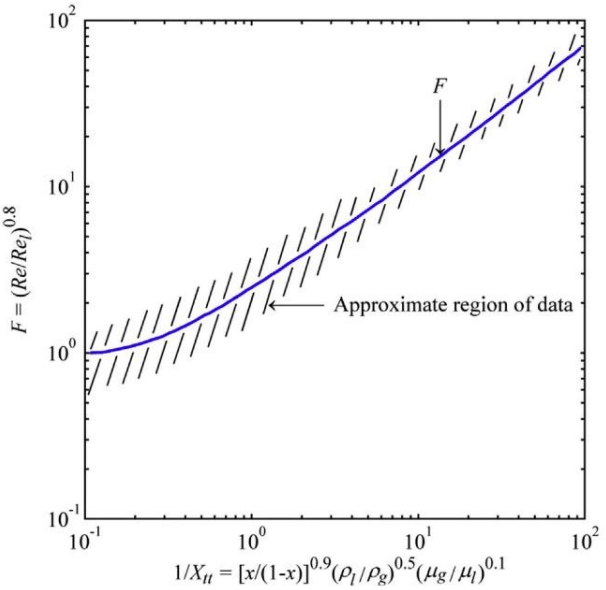

Fig. 2 Relationship between the dimensionless parameter $\hat{F}$ and the Martinelli coefficient (Chen & Fang 2014**)**

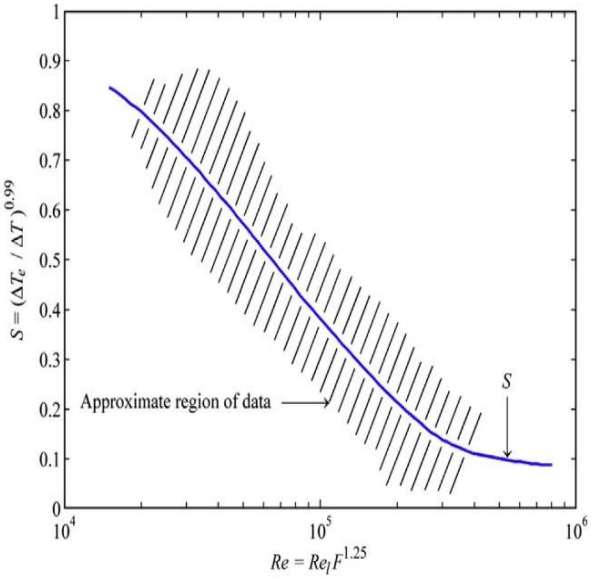

Fig. 3 An approximation for calculating the dimensionless parameter S (Chen & Fang 2014**)**

He offered Eq. (35) to compute the nucleate boiling heat transfer coefficient.

$$h_{NcB} = 0.00122\left[\frac{k_l^{0.79} c_{p_v}^{0.45} \rho_l^{0.49}}{\sigma^{0.5} \mu_l^{0.29} h_{lv}^{0.24} \rho_v^{0.24}}\right] \times \left[\Delta T_{sat}\right]^{0.24} \left[\Delta P_{sat}\right]^{0.75} S \quad (35)$$

Chen introduced Fig. 3 diagram to determine the S coefficient, which is the ratio of mean superheated temperature to wall superheated temperature, where $\Delta P_{sat} = P_{sat}(T_w) - P_l$ and $\Delta T_{sat} = T_{wall} - T_{sat}(P_l)$.

The optimal performance conditions with a mean error of 15% when the inlet fluid is water are $0.1 \prec P \prec 3.5\,MPa$, $0.06 \prec v \prec 4.48\,\frac{m}{s}$, $6.3 \prec q \prec 2400\,\frac{kW}{m^2}$, and $0.01 \prec x \prec 0.71$, based on the findings derived from Chen equations. As shown, appropriate results from these equations cannot be predicted for bubbly flow when the quality is less than 0.01.

3.3.2 Gungor and Winterton correlation

By enhancing Chen correlation and using 3693 data, Gungor and Winterton (1986) could obtain an equation for the heat transfer coefficient of two-phase flow in vertical and horizontal tubes that incorporates nucleate boiling and convective heat transfer. This correlation is commonly applied for refrigerants in a wide range of flow conditions, including boiling and condensation. The reported error for the Gungor & Winterton correlation is generally in the range of ±20% to ±40%, with some studies indicating the possibility of higher deviations under certain operational conditions (e.g., low or high pressure, or flow regimes that deviate from the laminar or fully turbulent flow).

Equations (36) to (38) show the correlation provided by them.

$$h_{tp} = Eh_l + \xi h_{NcB} \quad (36)$$

$$h_l = 0.023\left[\frac{G(1-x)D}{\mu_l}\right]^{0.8}\left[\frac{\mu c_p}{k}\right]_l^{0.4}\left[\frac{k_l}{D}\right] \quad (37)$$

$$h_{NcB} = 55P_r^{0.12}\left(-0.4343 LnP_r\right)^{-0.55} M^{-0.5} q^{0.67} \quad (38)$$

Equations (39) and (40) are used to derive coefficients E and ξ.

$$E = 1 + 24000Bo^{1.16} + 1.37(X_{tt}^{-1})^{0.86} \quad (39)$$

$$\xi = \left[1 + 0.00000115E^2\,\mathrm{Re}_f^{1.17}\right]^{-1} \quad (40)$$

The optimal performance conditions using Gungor and Winterton correlation to reach an acceptable range of error are $0.1 \prec P \prec 19.8\ MPa$, $2.95 \prec D \prec 25.4\ mm$, $4.7 \prec q \prec 2280\ \frac{kW}{m^2}$, $59.2 \prec G \prec 8179.3\ \frac{kg}{m^2 s}$, and $0 \prec x \prec 0.7$ [6].

4. GEOMETRY, BOUNDARY CONDITIONS AND IMPORTANT PARAMETERS IN NUMERICAL METHOD

Table 1 lists the tube geometric parameters, the pressure and saturation temperature that are being examined, as well as its mass flow rate and heat flux. The influence of gravity is also considered in this simulation.

At saturation temperature, liquid water is the first fluid to enter the tube. A constant mass flow rate serves as the problem inlet boundary condition, while a constant heat flux serves as the tube wall boundary condition. Pressure outlet has been applied as the outlet boundary condition

Table 1 Geometrical specifications and problem parameters

Fluid	Water
Tube material	Aluminum
Tube diameter	2 cm
Tube length	50 cm
Saturation temperature	425 K
Operational pressure	5 atm
Mass flow rate	0.05-0.1 kg/s
Heat flux	5-15 kW/m^2

since the fully developed condition is not guaranteed in this two phase flow. So, the pressure is fixed at the atmospheric pressure at the end of the tube.

The $\kappa-\omega$ turbulence model of shear stress transport (SST) was selected for flow modeling in this study to simulate turbulent flow conditions. There is a need for a turbulent model that, given the physical conditions of the problem, can simulate both the areas close to the wall and the areas distant from the wall since the phase change in the current problem occurs throughout the total area of the tube. The $\kappa-\omega(SST)$ model was selected as the final appropriate model for the current simulation because it employs a mixed function, using the $\kappa-\varepsilon$ model in the areas distant from the wall and the regular $\kappa-\omega$ model in the areas close to the wall.

It should be emphasized that to obtain the best results compared to the existing experimental correlations, various accessible turbulence models, such as the $\kappa-\varepsilon$ standard, RNG, realizable models, and standard $\kappa-\omega$ model as well as $\kappa-\omega(SST)$ model, were tested before choosing the $\kappa-\omega(SST)$ method as the final selected model.

As turbulence boundary conditions in the current modeling, the turbulence length scale and the intensity of the inlet flow have been determined, respectively, using Eqs. (41) and (42) under turbulent flow conditions.

$$l = 0.07D \tag{41}$$

$$I_t = 0.16\,\mathrm{Re}^{-1/8} \tag{42}$$

5. NUMERICAL SOLUTION PROCESS AND COMPUTATIONAL GRID

ANSYS Fluent software was used to perform numerical simulation for this study, transiently taking into account a time step of 0.0001s and a convergence criterion of 10^{-3}. Pressure based solver, which is commonly used in the modeling of two-phase flows and other problems involving low fluid flow velocity, is utilized in this work.

The coupled method has been used to solve the velocity and pressure equations simultaneously. The volume fraction equation has been discretized using the modified High Resolution Interface Capturing (HRIC) method, while the other equations have been discretized using the First-Order Upwind approximation. When calculating equations for pressure, momentum, volume fraction, turbulence kinetic energy, specific dissipation rate, turbulence viscosity, and energy, the under relaxation factors are considered 0.05, 0.05, 0.1, 0.1, 0.1, 0.1 and 0.05, respectively.

The axisymmetric two-dimensional model has been utilized to represent the fluid flow under the conditions of the current problem; because in the rising fluid flow in vertical tubes due to the impact of gravity, the changes of the two-phase flow regimes in the direction perpendicular to the plane are completely the same as its changes in the radial direction.

Additionally, the computational cell number has been raised near the wall to account for the impacts of the wall and the boundary layer and to improve the accuracy of the solution in these areas; conversely, at distances away from the wall, the grid density has been decreased to prevent an increase in calculation and time cost.

Several grids were tried to demonstrate grid independency in this study. Table 2 provides a brief presentation of some of these grids specifications. The problem was numerically solved using these grids separately, and the results for the maximum vapor volume fraction, wall temperature, and heat transfer coefficient are shown in Table 2.

While increasing the number of cells has a negligible effect on the vapor volume fraction and the wall temperature, the heat transfer coefficient was investigated to prove the independence of the computational grid in current study. The results confirm that the heat transfer coefficient doesn't change more than 0.88% when the numbers of elements are decreased from 125000 to 112500. Therefore, grid with 112,500 cells for half of the tube has been adopted as the approved grid in the problem.

6. VALIDATION

Validating a numerical solution against experimental data, as well as adjusting and readjusting the solution methods to get the least difference between the experimental results and numerical results, is one of the most crucial aspects of any numerical solution. Several experimental investigations have been undertaken in thissector over the last several decades due to the significance and use of the boiling process and phase change in thermodynamic cycles. The most reliable empirical correlations to compute the heat transfer coefficient were described in section 3.3.

In the current study, water with a saturation temperature of 425 K and a pressure of 500 kPa enters a vertical tube and rises against the direction of gravity. A constant heat flux applied to the wall causes the substance to change from liquid phase to vapor. A variety of heat flux values, from 5000 to 15000 W/m^2, were applied to the wall to examine the impact of these variations on the heat transfer coefficient. Conditions at the inlet, such as the Reynolds number of 17783, and the inlet fluid mass flow rate of 0.05 kg/s, are taken as constants. The findings of the numerical solution by the Eulerian boiling of RPI

Table 2 Mesh independence study

Grid	Number of cells	Heat transfer coefficient (W/m^2K)	Averaged wall temperature (K)	Maximum vapor volume fraction
1	80000	7815	426.353	0.9231
2	100000	7531	426.404	0.9185
3	112500	7394	426.438	0.9103
4	125000	7329	426.442	0.9091

Table 3 Comparing the results obtained by numerical solution and experimental correlations for heat transfer coefficient

Heat flux(W/m^2)	Heat transfer coefficient (W/m^2. K)		
	Numerical	Gungor & Winterton correlation	Chen correlation
5000	6117	4508	7759
10000	7395	5117	9933
15000	7508	6068	11510.9

Table 4 Comparing the results obtained by numerical solution and experimental correlations for wall temperature

Heat flux(W/m^2)	Wall temperature (K)		
	Numerical	Gungor & Winterton correlation	Chen correlation
5000	425.82	426.10	425.70
10000	426.43	426.95	426.00
15000	427.10	427.47	426.20

method were compared with the Gungor and Winterton (1986) and Chen (1966) correlations for wall heat transfer coefficient and wall temperature in this section. These results are shown in Tables 3, 4 and were determined based on the requirements of the current problem and the optimal performance conditions of the mentioned correlations. The presented results show the proper matching of the wall temperature results obtained with numerical solution and experimental correlations. In addition, results show that the heat transfer coefficient computed by numerical solution is in a good agreement with Gungor and Winterton (1986) and Chen (1966) correlations results of heat transfer coefficient within an averaged error of 34% and 27%, respectively. These correlations consider the effects of nucleate boiling and convective heat transfer at the same time, in contrast to those proposed by Shah (2006) and Kandlikar (1990). Furthermore, it should be noted that considering the possible inherent error of empirical correlations, the deviation of the numerical results from theses empirical results seems justified and reasonable.

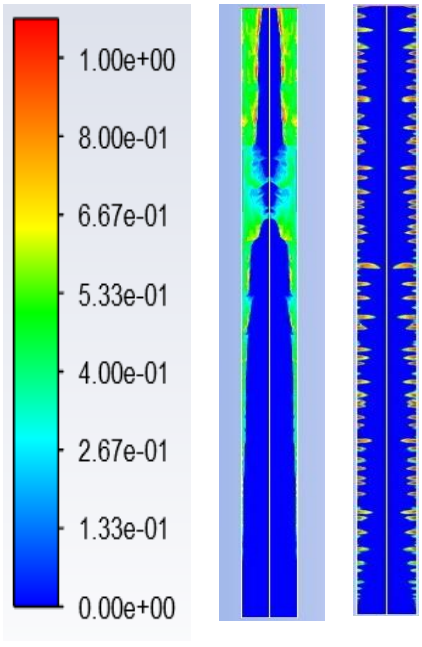

(a) **(b)**

Fig. 4 Initiation of the bubbly flow regime represented by the volume fraction contour of the vapor phase: (a) Eulerian RPI boiling model, and (b) Volume of Fluid (VOF) model

7. RESULTS AND DISCUSSION

7.1 Investigation and Comparison of the Bubbly Flow Regime Simulation with The Volume of Fluid (VOF) Model and RPI Boiling Model

Two numerical methods including VOF and RPI boiling using ANSYS FLUENT software were utilized to solve the current problem. The outputs were produced to observe the start of the bubbly flow regime formation with all physical and parametric conditions; including the inlet mass flow rate, the wall heat flux, tube dimensions, pressure, and other fluid properties; being the same in both models. These findings were obtained in around 4 days using the VOF model and 4 weeks using the RPI boiling model, indicating the RPI method larger computational cost. Figure 4 displays the results of the vapor phase volume fraction obtained by studied models. These results suggest that the numerical VOF model is more appropriate to depict the bubbly flow regime and the onset of the bubble formation process from the tube wall. This is true even though the RPI model can only show the created

Table 5 Comparing the results of VOF and RPI boiling numerical models with the experimental correlation results, Heat flux=15000 (W/m^2), mass flow rate 0.05 (kg/s)

	h (W/m^{2}K)	T_{wall}-T_{Sat}	x_{out}
RPI boiling model results	7508.22	2.1	0.00356
Error (%)	23.74	14.98	20.35
VOF model results	9632.08	2.01	0.00384
Error (%)	58.74	18.42	14.09

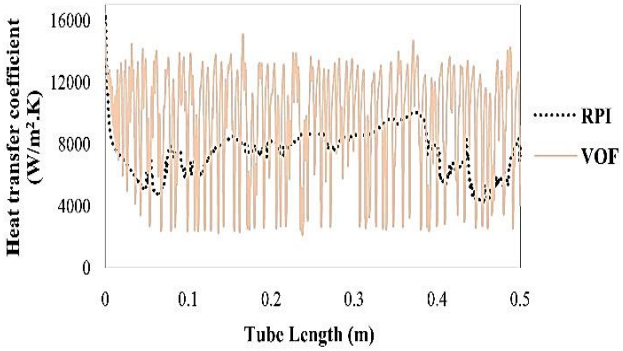

Fig. 5 Comparison of VOF and RPI boiling numerical model results for heat transfer coefficient

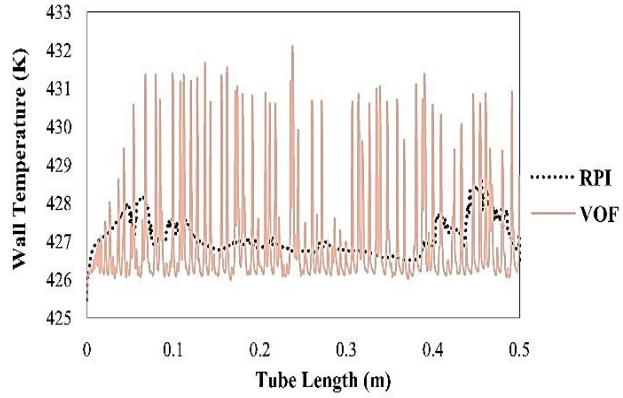

Fig. 6 Comparison of VOF and RPI boiling numerical model results for wall temperature

vapor phase and is unable to accurately distinguish the interface between the two phases.

7.2 Examining and Comparing the Boiling Heat Transfer Coefficient and Wall Temperature in the Bubbly Flow Regime by VOF and RPI Boiling Numerical Models

It is evident from analyzing the step-by-step problem solving using the two models of VOF and RPI boiling, that the VOF model solution process experiences significant oscillations because of the bubbles formation close to the wall and the resulting variation in the fluid properties. The RPI approach, however, significantly reduces these oscillations since bubbles cannot be detected precisely. Figures 5 and 6, respectively, display the heat transfer coefficient and the wall temperature.

Table 5 compares the numerical results of the averaged heat transfer coefficient, the outlet vapor phase quality, and the difference between the wall temperature and saturation temperature, with the Gungor and Winterton experimental correlation results and also represents the achieved error percentage. The temperature and heat transfer coefficient values obtained from the numerical solution using the RPI boiling model are more in line with the experimental results of the Gungor and Winterton (1986) correlations.

Since the RPI model predicts the heat transfer coefficient more accurately than the VOF model, it is selected as the primary numerical solution method in the continuation of the solution path to examine the impact of wall heat flux and inlet mass flow rate.

7.3 Investigating the Effects of Wall Heat Flux on The Bubbly Flow Using the RPI Boiling Model

Three distinct heat flux values were applied to the examined tube wall to investigate the impact of the wall heat flux on the bubbly flow heat transfer properties. This section examines the effects of heat flux modifications on outlet vapor quality, average wall temperature, and bubbly flow heat transfer rate; while the pressure, total mass flux, geometrical parameters, and other associated variables are considered constant.

7.3.1 The Influence of Wall Heat Flux on Vapor Quality

The wall heat flux increases the energy received by each computing cell filled with liquid phase, which turns into vapor phase if latent heat of the evaporation is gained.

More heat flux delivered to the wall results in more mass transfer to the vapor phase, which raises the vapor phase volume fraction throughout the process, accelerates the formation of bubbles on the wall surface and causes the vapor bubbles to grow faster once the process initiates.

The contour of the evaporation process of the water flow within the vertical tube is depicted in Fig. 7. At first, the saturated water flow enters the tube, and rises against the gravity. As can be seen in the figure, nucleation starts from the wall where the heat flux is applied. The process of bubble formation initiates faster and in a shorter length of the tube when the applied heat flux to the tube wall is increased. The least amount of vapor forms with a heat flux of 5000 W/m^2, and this is mostly on the wall side. When the heat flux is doubled, the quantity of generated vapor increases and tends to move toward the middle of the tube. As the heat flux is raised further, more vapor phase is formed and, as predicted, covers the whole side of the wall.

The mean and maximum volume fraction of the vapor phase in different heat fluxes are displayed in Table 6.

Table 6 Influence of wall heat flux on vapor volume fraction

Heat flux (W/m^2)	Maximum vapor volume fraction	Average vapor volume fraction
5000	0.821	0.266
10000	0.910	0.341
15000	0.940	0.438

Table 7 Influence of wall heat flux on the outlet vapor quality

Heat flux (W/m^2)	Vapor quality (Numerical results)	Vapor quality (Energy balance results)
5000	0.0009	0.00149
10000	0.00225	0.00298
15000	0.00356	0.00447

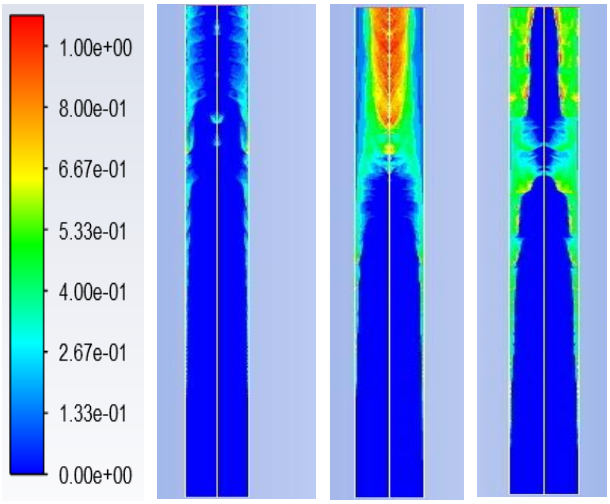

Fig. 7 Effect of increasing the wall heat flux on the volume fraction of the vapor phase (a: Heat flux=5000, b: Heat flux=10000 and c: Heat flux=15000 W/m^2)

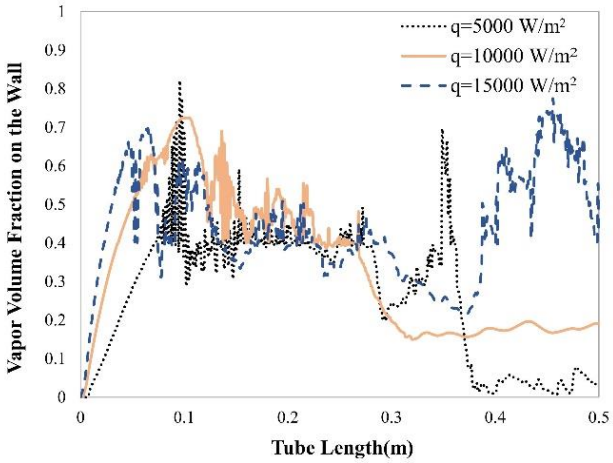

Fig. 8 Volume fraction of the vapor phase on the wall along the tube for different heat fluxes

Figure 8 displays the volume fraction of the vapor phase on the tube wall for varying heat fluxes. As the wall heat flux increases, a non-uniform behavior is shown in the graph and the volume fraction fluctuates more. Due to the type of the mechanism, complex behavior of the two-phase flow on the tube wall and the formation, growth and then movement of bubbles on the surface of the tube wall in different conditions, the volume fraction of vapor on the tube surface is completely fluctuating and changing. Therefore, this phenomenon may be caused by the rapid changes in how the liquid and vapor phases transform to each other, the unpredictable behavior of the vapor that forms on the surface, or the rapid changes in the fluid properties, particularly the thermal conductivity coefficient. So, the mean values of the two-phase flow properties are significant because the tube wall is adjacent to a mixture of liquid and vapor phases. The volume fraction of the vapor phase on the wall can be observed to decrease near the tube outlet, indicating the bubbles propensity to move toward the center of the tube and unite to create the slug flow regime. The volume fraction decreases at a flux of 5000 W/m^2 more than other fluxes. However, at higher heat fluxes (15,000 W/m^2), the amount of formed vapor is such that it can fill the entire surface of the tube and even near the wall and therefore, the increase in the volume fraction of the vapor phase on the wall at the end of the tube is for this reason.

The quality of the outlet vapor phase at various heat fluxes is reported in Table 7. These numerical results have been compared with the energy balance results. Consequently, in the bubbly flow regime, the quality of the outlet vapor, the volume fraction of the vapor phase, and the oscillations in the volume fraction diagram, increase by increasing the wall heat flux. Thus, the outlet vapor quality improved to approximately 2.5 times in comparison with the initial value, with a 100% increase in the wall heat flux, and this rise reached approximately four times the initial value with a further increase in the heat flux up to 15000 W/m^2.

7.3.2 The influence of Wall Heat Flux on Wall Temperature

When a constant heat flux is applied to the wall, the inlet fluid temperature rises progressively over the saturation temperature and as a result of the forced convection on the surface, the wall temperature rises steadily. In other words, the internal energy of the liquid phase and its temperature rise along the tube length; that is, the greater the heat flux delivered to the wall, the higher the energy absorbed by each cell occupied by the saturated

Table 8 Effect of wall heat flux on wall temperature difference with saturation temperature

Heat flux (W/m^2)	Temperature difference with saturation temperature		
	Empirical correlation (Gungor and Winterton, 1986)	Numerical solution	Error (%)
5000	1.10	0.82	25.4
10000	1.95	1.43	26.7
15000	2.47	2.10	15

Table 9 Influence of wall heat flux on the heat transfer coefficient

Heat flux (W/m^2)	Numerical results	Empirical correlation results		Error (%)
5000	6117	Chen	7759	21.1
		Gungor & Winterton	4507.9	35.7
10000	7394.65	Chen	9933	25.5
		Gungor & Winterton	5117.1	44.5
15000	7508.22	Chen	11510.9	34.8
		Gungor & Winterton	6067.7	23.7

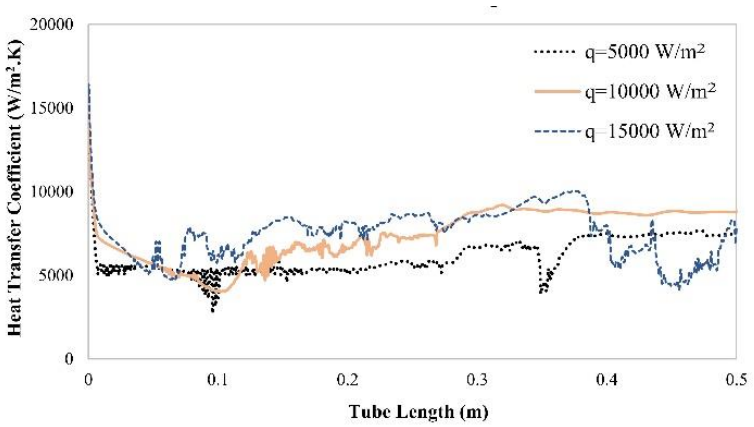

Fig. 9 Two-phase heat transfer coefficient along the tube for different heat fluxes

liquid. Table 8 represents the average wall temperature difference in proportion to the inlet fluid temperature, both numerically and by the Gungor and Winterton (1986) experimental correlation at varying heat fluxes.

Results indicate that raising the heat flux from 5000 to 10000 W/m^2 increases the wall temperature about 0.57 degrees, and raising the heat flux to 15000 W/m^2 increases the wall temperature by 1.24 degrees. Numerical results are compared with empirical correlation results of Gungor and Winterton (1986), and the error percentage of the findings is given.

7.3.3 The influence of Wall Heat Flux on the Heat Transfer Coefficient

The two-phase heat transfer coefficient increases gradually as the wall heat flux increases, as observed by the numerical results displayed in Table 9. Indeed, the quantity of generated bubbles and the flow turbulence increase with the increasing of heat flux applied to the wall. It is worth noting that these reported values are the mean value of the two-phase heat transfer coefficient. Based on the baseline value of 5000 W/m^2, the results indicate that the average two-phase heat transfer coefficient improves by 21% and 23%, respectively, when the wall heat flux is doubled or tripled. This illustrates how the bubbles affect the bubbly flow. The results of all numerical solutions are compared with empirical correlations, and Table 9 displays the errors.

The heat transfer coefficient increases as a result of the intensification of the flow turbulence caused by the increased number of generated bubbles that emerge as the heat flux delivered to the wall increases from 5000 to 10000 W/m^2, as seen in Fig. 9. Nevertheless, the convection effect overcomes the effects of bubble formation and bubble turbulence until the heat flux reached 15000 W/m^2, due to the rise in flow bubbles caused by the density reduction and gravity and vapor coverage near the wall. Therefore, the two-phase heat transfer coefficient has suddenly decreased, because the vapor heat transfer coefficient is significantly lower than the liquid heat transfer coefficient.

The complex behavior of the two-phase flow on the tube wall is the primary reason of the fluctuations can be seen on various parameters. Thus, variations in fluid velocity have been brought about by the production of vapor bubbles and the peculiar behavior of the vapor that developed on the tube surface. It is impossible to pinpoint the precise location of the liquid phase on the tube wall surface due to the irregular growth and departure of the vapor bubbles from the wall. Indeed, the primary cause of the variations and instability observed on the surface is the change in properties, especially the thermal conductivity

Table 10 Influence of inlet mass flow rate on the outlet vapor quality

Mass flow rate (kg/s)	Vapor quality (Numerical)	Vapor quality (Empirical correlation)	Error (%)
0.05	0.00275	0.00372	26
0.075	0.00176	0.00248	29.2
0.1	0.00127	0.00186	29.8

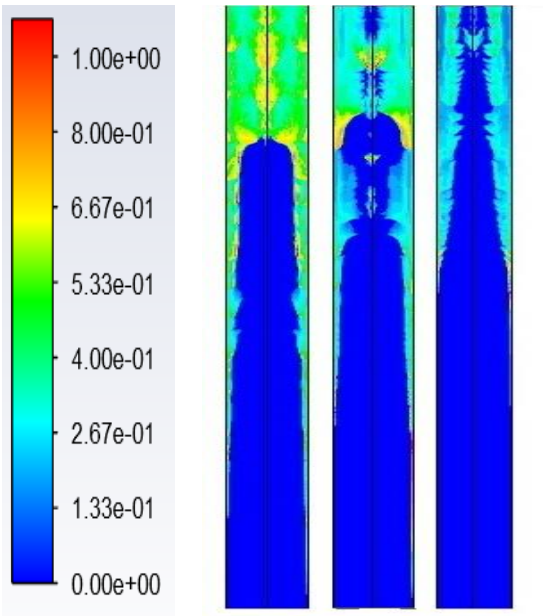

Fig. 10 Effect of increasing the inlet mass flow rate on the volume fraction of the vapor phase (a: Mass flow rate=0.05, b: Mass flow rate =0.075 and c: Mass flow rate =0.1 kg/s)

coefficient, between the liquid and vapor phases. Particularly, where the liquid phase forms, there is a rise in thermal conductivity, and where the vapor phase forms, there is a drop in thermal conductivity. So, the mean values of the two-phase flow properties are significant because the tube wall is adjacent to a mixture of liquid and vapor phases.

7.4 Investigating the Effects of Inlet Mass Flow Rate on the Bubbly Flow Using the RPI Boiling Model

7.4.1 Influence of the Inlet Mass Flow Rate on Vapor Quality

Based on Fig. 10, which depicts the contour of the volume fraction of the vapor phase for various mass flow rates in a vertical tube with a specific length, it can be seen how the vapor phase varies. The figure makes it evident that when the inlet mass flow rate increases, the nucleate boiling zone length grows and the two-phase convective heat transfer zone forms more slowly.

Table 10 shows that the quality of the vapor phase reduced by about 36% when the mass flow rate increased from 0.05 to 0.075 kg/s (a 50% increase) and the percentage of vapor phase deterioration reached 54% when the mass flow rate increased to 0.1 kg/s (a 100% increase).

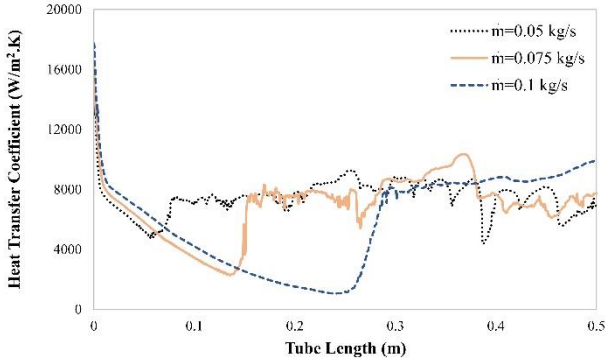

Fig. 11 Convective heat transfer coefficient along the tube for different mass flow rates

7.4.2 Influence of Inlet Mass Flow Rate on the Heat Transfer Coefficient

The impact of mass flow rate on the heat transfer coefficient along the tube length is shown in Figure 11. The heat flux applied to the wall is fully used to raise the wall temperature and consequently the temperature difference between the wall and the saturation temperature, at the beginning of the flow and before the bubble formation. As a result, the two-phase heat transfer coefficient decreases as the temperature difference in a constant heat flux increases. It is obvious that with larger mass flow rate, the drop in the heat transfer coefficient persists for a longer length of the tube, given that the bubble formation process from the wall side is delayed. After this region, the formation of bubbles and the subsequent variations caused by bubble turbulence, quickly lead to an increase in the heat transfer coefficient. Accordingly, abrupt changes in the fluid properties near the wall, particularly the shift in the thermal conductivity coefficient, are the cause of the observed variations.

8. CONCLUSION

In this study, the Eulerian-Eulerian approach was used to simulate the bubbly flow regime, which includes vapor bubbles in the rising water flow within a vertical tube, considering the mass transfer resulting from phase change in saturated boiling. In order to identify the optimal numerical model and the extent of application of available numerical models in the simulation of bubbly flow, volume of fluid model (VOF) and Eulerian boiling model of Rensselaer Polytechnic Institute (RPI) were compared and evaluated. Based on this investigation, the following conclusions were obtained:

- By comparing the modeling results of two boiling RPI and VOF models, it was discovered that the chosen

RPI boiling model computes the heat transfer coefficient, approximately 35% closer to the results of the empirical correlation of Gungor and Winterton (1986) than the VOF model. However, compared to the RPI model, the numerical method of VOF is better able to depict the bubbly flow regime and bubble formation process from the tube wall with a less computational cost. Therefore, the combination of the VOF method for precise phase interface tracking and the RPI boiling model for simulating bubble dynamics and heat transfer mechanism makes these models well-suited for bubbly flow simulations in two-phase regimes, particularly in boiling systems where both interface tracking, bubble dynamics and heat transfer are critical to the accuracy of the simulation.

- The findings of the numerical simulation showed that when the wall heat flux increases, the temperature of the tube wall and the quality of the outlet vapor rise steadily. Additionally, nucleation and vapor bubbles formation begin at a shorter tube length.
- The convective heat transfer coefficient, wall temperature, and vapor volume fraction oscillations increased by increasing the wall heat flux. The abrupt changes in the fluid properties close to the wall, particularly the shift in the thermal conductivity coefficient, were the primary cause of these oscillations.
- An average error of 34.6 and 27.1 percent, respectively, were observed when comparing the results of the Eulerian RPI boiling numerical model with the correlations of Gungor and Winterton (1986) and Chen (1966) for the heat transfer coefficient of the bubbly flow in three distinct heat fluxes.
- A 100% increase in the wall heat flux relative to its original value of 5000 W/m^2, resulted in a 2.5-fold increase in the outlet vapor quality, a 75% rise in the temperature difference between the wall and the saturation temperature, and a 20.8% increase in the average wall heat transfer coefficient.
- A rapid decline in the heat transfer coefficient occurred near the end of the tube at a high heat flux of 15000 W/m^2, as a result of the amount of produced vapor covering the side of the wall and its motion towards the end of the tube due to the gravity and density difference.
- The nucleate boiling zone at the flow entrance grew longer due to an increase in mass flow rate, and the two-phase convective heat transfer zone formed more slowly.
- A 50% increase in the inlet mass flow rate resulted in a 36% reduction in vapor phase quality and with a 100% increase in mass flow rate, the vapor phase quality dropped about 54%.
- It was shown that the bubble generation process from the wall was delayed when the inlet mass flow rate was increased. Before the formation of the bubbles and nucleate boiling initiation, the heat flux given to the wall was employed to raise the temperature of the wall. The increasing of wall temperature causes a drop in the two-phase heat transfer coefficient at a constant heat flux. Hence, with a larger mass flow rate, the decrease in the heat transfer coefficient persists over a longer length of the tube since the heat flux is constant. Furthermore, a rise in the heat transfer coefficient was observed in conjunction with the bubbles formation and the bubble induced turbulence.

Thus, simulating bubble formation and dynamics and the estimation of heat transfer coefficient in bubbly flow two-phase regime within the evaporators with vertical tubes can be precisely studied with the aid of the current research findings.

CONFLICT OF INTEREST

The authors declare that they have no conflict of interest.

AUTHORS CONTRIBUTION

S. Torfeh and **M. Mirzaei** performed numerical simulation, project investigation and validation. They also wrote the manuscript. **R. Kouhikamali** examined the manuscript and supervised all the work of the article.

REFERENCES

Anderson, T. B., & Jackson, R. (1967). A fluid mechanical description of fluidized beds, *Industrial & Engineering Chemistry Fundamentals, 6*, 527-534. https://doi.org/10.1021/i160024a007

ANSYS FLUENT, User's Guide (Release 18.2). ANSYS Inc, (2017).

Attarakih, M., Hasseine, A., & Bart, H. J. (2016). CFD modelling of bubbly gas flow using coupled OPOSPM-two-fluid model. *Computer Aided Chemical Engineering, 38*, 403-408. https://doi.org/10.1016/B978-0-444-63428-3.50072-2

Azadbakhti, R., Pourfattah, F., Ahmadi, A., Akbari, O., & Toghraie, D. (2020). Eulerian – Eulerian multi-phaseRPI modeling of turbulent forced convective of boiling flow inside the tube with porous medium. *International Journal of Numerical Methods for Heat & Fluid Flow*, *30*(5), 2739-2757. https://doi.org/10.1108/HFF-03-2019-0194

Bowen, R. M. (1976). *Theory of mixtures, volume 3 of continuum physics, mixtures and em field theories.* Academic Press, Cambridge, Chapter 2, 1-127.

Chen, J. C. (1966). Correlation for boiling heat transfers to saturated fluids in convective flow. *Industrial & Engineering Chemistry Process Design and Development*, *5*(3), 322-329. https://doi.org/10.1021/i260019a023

Chen, W., & Fang, X. (2014). A note on the Chen correlation of saturated flow boiling heat transfer.

International Journal of Refrigeration, *48*, 100-104. https://doi.org/10.1016/j.ijrefrig.2014.09.008

Collier, J. G., & Thome, J. R. (1996). *Convective Boiling and Condensation*. Oxford engineering science series. https://doi.org/10.1017/S0022112095233160

Etminan, A., Muzychka, Y. S., & Pope, K. (2021a). Film thickness and pressure drop for gas-liquid taylor flow in microchannels. *Journal of Fluid Flow, Heat and Mass Transfer*, *8*, 60-71. https://doi.org/10.11159/jffhmt.2021.008

Etminan, A., Muzychka, Y. S., & Pope, K. (2021b). Liquid film thickness of two-phase slug flows in capillary microchannels: A review paper. *The Canadian Journal of Chemichal Engineering*, 1-24. https://doi.org/10.1002/cjce.24068

Gungor, K. E., & Winterton, R. H. S. (1986). A general correlation for flow boiling in tubes and annuli", *International Journal of Heat and Mass Transfer*, *29*, 351-358. https://doi.org/10.1016/0017-9310(86)90205-X

Hasanpour, B., Irandoost, M. S., Hassani, M., & Kouhikamali, R. (2018). Numerical investigation of saturated upward flow boiling of water in a vertical tube using VOF model: effect of different boundary conditions. *Heat and Mass Transfer*, *54*(2), 1925–1936. https://doi.org/10.1007/s00231-018-2289-3

Hirt, C. W., & Nichols, B. D. (1981). Volume of fluid (VOF) method for the dynamics of free boundaries. *Journal of Computational Physics*, *39*(1), 201-225. https://doi.org/10.1016/0021-9991(81)90145-5

Igaadi, A., Mghari, H. El., & Amraoui R. El. (2023). Computational analysis of subcooled flow boiling in a vertical minichannel with two different shapes under various mass fluxes. *Journal of Applied Fluid Mechanics*, *16*(10), 2069-2081. https://doi.org/10.47176/jafm.16.10.1787

Kandlikar, S. G. (1990). A general correlation for saturated two-phase flow boiling heat transfer inside horizontal and vertical tubes. *Journal of Heat Transfer*, *112*(1), 219-228. https://doi.org/10.1115/1.2910348

Kandlikar, S. G. (1999). *Handbook of Phase Change: Boiling and Condensation (1st ed.)*. Routledge. https://doi.org/10.1201/9780203752654

Kural, N., & Podowski, M. (1991). *On the modeling of multidimensional effects in boiling channels.* Proceedings of 27th National Heat Transfer Conference, Minneapolis, 30-40.

Laviéville, J., Boucker, M., Quémérais, E., Mimouni, S., & Méchitoua N. (2006). *NEPTUNE CFD V1.0 Theory Manual*, EDF.

Lim, Y. S., & Yu, S. C. M. (2014). Numerical simulations of heat transfer characteristics of gas-liquid two phase flow in microtubes. *International Journal of Thermal Sciences*, *84*, 115-124. https://doi.org/10.1016/j.ijthermalsci.2014.07.001

Mizushina, T., Ito, R., & Miyashita, H. (1968). Characteristics and methods of thermal design of evaporative coolers. *Chemical Engineering*. *32*(1), 55-61. https://doi.org/10.1252/kakoronbunshu1953.32.55

Monferrer, C. P., Andreu, G. M, Chiva, S., Cuenca, R. M., & Muñoz-Cobo, J. L. (2018). A CFD-DEM solver to model bubbly flow. Part I: Model development and assessment in upward vertical pipes. *Chemical Engineering Science*, *176*, 524-545. https://doi.org/10.1016/j.ces.2017.11.005

Mughal, M. U. K., Waheed, K., Sadiq, M. I., Molla, A. H., Harun, Z., & Etminan, A. (2024). Water flow boiling in micro/mini channels using volume of fluid model. *Applied Sciences*, *14*, 759. https://doi.org/10.3390/app14020759

Pang, M., Wei, J., Yu, B. (2010), Numerical study of bubbly upflows in a vertical channel using the Euler-Lagrange two-way model. *Chemical Engineering Sciences*, *65*, 6215-6228. https://doi.org/10.1016/j.ces.2010.09.008

Shah, M. M. (1982). Chart correlation for saturated boiling heat transfer: equation and further study. *ASHRAE Transactions*, *88*(1), 185-196.

Shah, M. M. (2006). Evaluation of general correlations for heat transfer during boiling of saturated liquids in tubes and annuli. *American Society of Heating and Air-conditioning Engineers*, *12*(4), 1047-1063. https://doi.org/10.1080/10789669.2006.10391450

Son, G. (2001). A numerical method for bubble motion with phase change. *An International Journal of Computation and Methodology*, *39*(5), 509-523. https://doi.org/10.1080/104077901750188868

Torfeh, S., & Kouhikamali, R. (2015). Numerical investigation of mist flow regime in a vertical tube. *International Journal of Thermal Sciences*, *95*, 1-8. https://doi.org/10.1016/j.ijthermalsci.2015.03.015

Wu, Z., Qian, X., Peng, X., Song, Y., Song, W., Song, F., & Liu, P. (2023). Modeling of subcooled flow boiling for hypervapotron in divertor of fusion reactor based on RPI model. *Case Studies in Thermal Engineering*, *49*, 103289. https://doi.org/10.1016/j.csite.2023.103289

Yang, H., Xue, J., Li, L., Li, X., Lin, P., & Zhu, Z. (2022). Modeling of bubbly flow using a combined volume of fluid and discrete bubble model: investigation on interphase forces. *Journal of Applied Fluid Mechanics*, *15*(3), 843-855. https://doi.org/10.47176/jafm.15.03.33280

Ye, T., Shyy, W., & Chung J. N. (2001). A fixed-grid, sharp-interface method for bubble dynamics and phase change. *Journal of Computational Physics*, *174*(2), 781-815. https://doi.org/10.1006/jcph.2001.6938

Zhang, C., Chen, L., Qin, F., Liu, L., Ji, W. T., & Tao, W. Q. (2023). Lattice Boltzmann study of bubble dynamic behaviors and heat transfer performance

during flow boiling in a serpentine microchannel. *Applied Thermal Engineering*, *218*, 119331. https://doi.org/10.1016/j.applthermaleng.2022.119331

Zhang, X., Wang, J., & Wan, D. (2020). An improved multi-scale two phase method for bubbly flows. *International Journal of Multiphase Flow*, *133*, 103460. https://doi.org/10.1016/j.ijmultiphaseflow.2020.103460

Zhou, Z., Wang, S., He, J., Ke, H., Lin, M., & Wang, Q. (2023). Bubble dynamics and heat transfer characteristics of flow boiling in a single pentagonal rib channel. *ASME Journal of Heat And Mass Transfer*, *145*(1), 011602. https://doi.org/10.1115/1.4056067